NMR Imaging of Flow Velocity in Porous Media

C. T. Philip Chang and A. Ted Watson
Dept. of Chemical Engineering, Texas A&M University, College Station, TX 77843

Two NMR velocity imaging methods based on the pulsed field gradient stimulated-echo technique are evaluated for the measurement of fluid flow in porous media. The spatial resolution and dynamic scale of velocity imaging experiments are chosen to represent the macroscopic behavior of the complex motion of fluid molecules. A theoretical formulation for data interpretation is presented and demonstrated with experimental data for water flow in a glass-bead pack and sandstone samples. Velocity imaging methods investigated include the use of flow-induced phase shifts and the measurement of spatially resolved velocity distributions. The results show that the phase-shift method is not suitable for some porous media. By contrast, the measurement of spatially resolved velocity distributions not only allows a map of mean velocity to be determined, but also provides information about the velocity field within each elemental volume of the image.

Introduction

A large variety of processes of interest to industry and society involve the flow of fluids through porous media. Examples include the use of filtration to purify water and treat sewage, membranes to separate gases, and chemical reactors having porous catalyst supports. A common goal is often the development of the means of mathematically model flow in porous media in order to effectively design and control the processes.

We direct our attention to the flow of fluids in media characteristic of underground sedimentary porous media; this process is of great interest for petroleum recovery and groundwater remediation, to name two applications. The primary method for mathematically describing such processes is macroscopic representations in which state variables are based on representative volume elements, or local volume averages (Bear, 1975; Slattery, 1981). In some situations, such as the creeping flow of a single fluid phase in porous media, the mathematical model (i.e., Darcy's law) is well supported. Even in this situation, however, the media properties—the porosity and permeability—are locally defined, and thus spatially dependent, and must be determined in order to effectively use the model for prediction. The presence of multiple fluid phases greatly complicates the situation. While simulations of two-phase flow in porous media have been carried out for a number of years, the theoretical and experimental bases for the extension of the Darcy model has not been so firmly established, and questions remain regarding the functional dependence of properties, such as the relative permeabilities (Kulkarni et al., 1998). In particular, the description of multiphase flow in heterogeneous media has hardly been addressed. There are many more important and complex processes for which models have not been developed, or have been proposed but never validated. For example, the modeling of biological processes within porous media would seem to be in its infancy.

Research into flow in porous media has been severely limited by our experimental capabilities. By and large, experiments have been analyzed on the basis of measurements made *outside* of the sample of interest. The actual flow behavior within the sample has largely remained unknown. In recent years, X-ray computed tomography (CT) and nuclear magnetic resonance (NMR) imaging have provided unprecedented opportunities for determining information corresponding to local regions within porous media. When fully developed, these modalities will substantially enhance our abilities to understand and describe flow in porous media.

The characteristic measurement with CT scanning that is useful for probing processes in porous media is the discernment of local densities. With suitable experimentation, CT scanning can be used to characterize properties associated

Correspondence concerning this article should be addressed to C. T. P. Chang.

with the *storage* of fluids, such as porosity, fluid saturations, and adsorption isotherms (Lu et al., 1994).

Nuclear magnetic resonance imaging (MRI) is a much more versatile tool than CT scanning; it can potentially provide even greater information. The primary development of MRI has been as a diagnostic tool within the medical field. While those techniques can be used to visualize fluid states in a porous medium, such applications provide little information that will enhance our understanding of flow in porous media. However, a variety of experiments can be devised to probe a number of different molecular events, and suitable design and analysis of such experiments can provide important information for characterizing fluids and flow in porous media.

We consider here properties useful for describing flow at the macroscopic scale. Methodologies have been developed so that the amounts of fluid phases corresponding to imaged voxels can be determined, providing for determination of fluid saturation and porosity distributions (Watson and Chang, 1997). The size of the voxel can be selected as part of the experimental imaging sequence, but current maximum resolutions for sedimentary porous media are on the order of 100 μm^3. These properties can be represented as volume averages over regions containing many pores, and thus represent macroscopic properties.

MRI can also be used to directly observe the movement of molecules associated with diffusion or flow. This provides for a unique opportunity to determine noninvasively local velocities within porous media. Suitably analyzed, one can obtain permeability distributions, or basic information about the flow of multiple fluid phases.

There have been relatively few studies regarding velocity imaging in porous media. Most of the studies have applied standard techniques and analyses developed for observing flow systems in conduits (Gleeson and Woessner, 1991; Merrill, 1994), or designed experiments for use with model porous media containing pores sufficiently large so that those standard techniques can be suitable used (Callaghan et al., 1992; Nesbitt et al., 1992; Kutsovsky et al., 1996). Other studies have presented the experimental results in terms of the probability distribution for the displacement of fluid molecules (Lebon et al., 1996; Packer and Tessier, 1996; Tessier et al., 1997), but have not related the results to spatially resolved characteristics of the media or process.

Here, we report on the use of MRI for determining spatially resolved macroscopic velocity distributions. A theoretical formalism for data interpretations, which was derived from basic pulsed field gradient (PFG) NMR imaging principles, is outlined in the following section. The methods are demonstrated using data obtained for flow through a bead pack and sandstone sample.

Methodology

PFG NMR detects molecular displacement over a well-defined time period and can be an excellent approach to the characterization of transport processes as well as structural features in porous media. The imaging of the velocity of fluid molecules can be achieved by using the PFG method to encode the displacement of fluid molecules and coupling this with a suitable NMR imaging sequence. Due to the complex nature of molecular motion in the pore space, naive assumptions about the interpretation of the measurement process may lead to an incorrect characterization of the flow process. In this section, we derive expressions for data interpretation from basic PFG imaging principles.

Pulsed field gradient NMR imaging

In simple NMR imaging, spatial information is obtained by introducing a time-dependent spatially linear magnetic-field gradient $g(t)$ so that the oscillating frequency of the transverse magnetization varies across the sample as

$$\omega'(r) = \gamma g \cdot r. \tag{1}$$

The acquired signal has the form (Callaghan, 1991):

$$S(k) = \int \rho(r) \exp(ik \cdot r)\, dr, \tag{2}$$

where

$$k = \gamma \int_0^t g(t')\, dt', \tag{3}$$

and $\rho(r)$ is the spin density as a function of spatial coordinate r. The gyromagnetic ratio γ is a known constant for a given nucleus. The Fourier relationship between the measured signal and the spin density forms the basis for NMR imaging.

The phase of the NMR signal can also be made sensitive to molecular translational motion. The use of phase shifts of the transverse nuclear magnetization to measure molecular velocity has been investigated for decades, and its potential application to the spatially resolved measurement of flow velocity was first suggested by Moran (1982). The measurements of molecular translation involve two primary elements. The first element is the use of a pulsed magnetic field gradient to impose phase shifts on the moving spins. The second is the use of spin echoes to detect the effects of phase shifts on the NMR signals. The actual movements of fluid molecules through a porous medium is expected to be irregular spatially and temporally. To obtain a measure of the molecular displacement during a well-defined time period, it is advantageous to apply the gradients in the form of two intense gradient pulses separated by a time interval that is much longer than the pulse duration. The two identical pulses are applied during the dephasing and rephasing periods of a spin-echo sequence. For stimulated-echo experiments, gradient pulses are inserted in the transverse evolution periods. Figure 1 shows the incorporation of the velocity-encoding field gradient pulses in the stimulated-echo imaging pulse sequence that was used in this work. The spatial information for imaging is phase-encoded in the x-direction and frequency-encoded in the z-direction. The time Δ between the velocity-encoding gradient pulses is the time during which fluid molecules are tracked. A remarkable feature of the stimulated echo is that the relaxation decay has a T_1 dependence during the interval between the second and third RF pulses. Longer observation time Δ is allowed without the usual signal attenuation due to T_2 relaxation, since T_1 is usually much longer than T_2 for

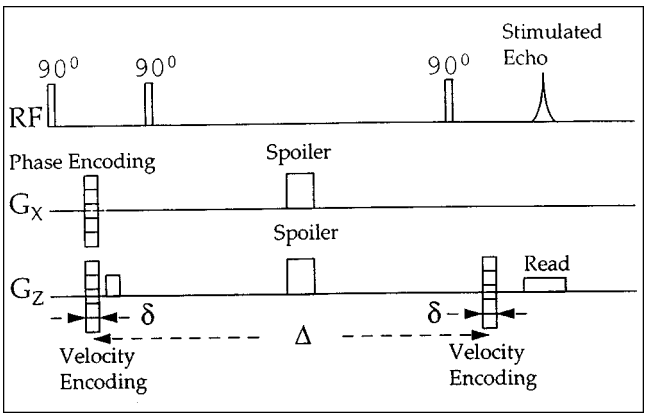

Figure 1. Stimulated-echo pulse sequence for projection imaging in the *x*-*z* plane of the *z*-component of the velocity.

The two spatial dimensions are phase encoded in the *x*-direction and frequency encoded in the *z*-direction, respectively. The velocity encoding is done in the *z*-direction by varying the amplitude of the velocity-encoding gradient pulses.

fluids in porous media. The water-saturated sandstone sample used in this work has relaxation times of $T_1 \approx 600$ ms and Hahn spin-echo $T_2 \approx 15$ ms.

Now consider the effect of the two velocity-encoding gradient pulses of amplitude G, pulse width δ, and separation Δ. According to Eq. 1, the phase shift induced by a spin at time t following the path $r(t')$ in a gradient $g(t')$ is given by

$$\phi(t) = \gamma \int_0^t g(t') \cdot r(t')\, dt'. \tag{4}$$

In the narrow-pulse approximation, where $\delta \ll \Delta$, the pulse duration δ is assumed short enough so that negligible molecular displacement occurs during this period compared to that during Δ. The first pulse imparts a phase shift $\gamma\delta G \cdot r_0$ to a spin located at r_0. This phase shift is inverted by the last two 90° pulses in the stimulated-echo sequence. Suppose that the spin has moved to position $r_0 + R$ at the time of the second gradient pulse. Then, the net phase shift for the spin is $\gamma\delta G \cdot R$. As in Eq. 3, it is convenient to introduce another wave vector q, given by

$$q = \gamma\delta G, \tag{5}$$

to describe the phase modulation due to molecular motion. While k is conjugate to the spin position r, q is conjugate to the spin displacement R.

By combining the velocity encoding gradients and static imaging, it is possible to obtain a distribution function of spin translation in individual voxels of the sample. We generalize the spin density $\rho(r)$ to a spatially-displacement joint density function (Moran, 1982) defined as

$$\rho_\Delta(r, R) = \rho(r) P'_\Delta(R, r), \tag{6}$$

where $P'_\Delta(R, r)$ is the normalized distribution function of spin displacement over a period of time Δ for a voxel at location r, satisfying the normalization condition, $\int P'_\Delta(R, r) dR = 1$. The relaxation effects are included in the definition of $\rho_\Delta(r, R)$. The joint density function $\rho_\Delta(r, R)$ is proportional to the number of spins per unit spatial volume and per unit displacement volume, at location r, with displacement R during Δ. The measured NMR signal is modulated by the two wave vectors, k and q, and can be written, like Eq. 2, as

$$S(k, q) = \int\int \rho_\Delta(r, R) \exp(ik \cdot r) \exp(iq \cdot R)\, dr\, dR. \tag{7}$$

Hence, the joint density function for a voxel can be reconstructed by Fourier transforming the NMR signal with respect to k and q.

Velocity imaging

The time average of each spin's velocity in the direction of the gradient, for example, z-direction, is defined as

$$\bar{v} = \frac{Z}{\Delta}, \tag{8}$$

where $Z = z(\Delta) - z(0)$ is the displacement in the z-direction. The NMR signal for a voxel at position r is the Fourier transformation of Eq. 7 with respect to k, and is calculated as

$$\begin{aligned} S'(r, q) &= \rho(r) \int_{-\infty}^{\infty} P'_\Delta(Z, r) \exp(iqZ)\, dZ \\ &= \rho(r) \int_{-\infty}^{\infty} P_\Delta(\bar{v}, r) \exp(iq\bar{v}\Delta)\, d\bar{v}, \end{aligned} \tag{9}$$

when the relationships in Eq. 6 and Eq. 8 are used. The velocity distribution function $P_\Delta(\bar{v}, r)$ is the probability density of spins that are moving within the velocity range $\bar{v}$ and $\bar{v} + d\bar{v}$. The ensemble averaged velocity for a voxel is given by

$$\langle \bar{v} \rangle_r = \int_{-\infty}^{\infty} \bar{v} P_\Delta(\bar{v}, r)\, d\bar{v}. \tag{10}$$

In this work two methods to estimate the mean velocity for each voxel were investigated: (1) the phase-shift, and (2) the velocity-distribution. The first method uses the phase of the measured NMR signal in Eq. 9 to estimate the mean velocity. Since the phase of the NMR signal is very sensitive to the inhomogeneity in the magnetic field, a reference phase map at zero velocity is required to correct for any phase errors caused by the field inhomogeneity (Caprihan et al., 1990a), which may arise from the magnet shimming, susceptibility effects, and eddy currents due to gradient switching. In the second method, the velocity distribution function $P_\Delta(\bar{v}, r)$ is measured and Eq. 10 is used to calculate $\langle \bar{v} \rangle_r$. The velocity distribution function is determined by performing the inverse Fourier transform of the NMR signal in Eq. 9 with respect to q. To do this, the NMR data set is acquired with regularly increased gradient amplitude G. The phase errors are eliminated by calculating the magnitude of the Fourier-transformed complex array. The reliability, advantages, and disadvantages of these methods are discussed later.

Results and Discussion

Experiments were performed using a General Electric 2T Omega CSI system with an Oxford instrument superconducting magnet with a 31-cm-diameter horizontal bore. Magnetic field gradients of up to 20 G/cm were provided by a shielded Acustar gradients set. A 4.4-cm ID birdcage RF resonator was used for both radiofrequency transmission and reception of the NMR signal.

The stimulated-echo pulse sequence for imaging the *z*-component of the flow velocity in the *x*-*z* plane is shown in Figure 1. A similar sequence with the slice-selective RF excitation and minor modifications was used to obtain cross-sectional images of the *z*-component velocity. The velocity encoding is done by varying the amplitude of the velocity encoding gradient pulses, which were applied along the direction of the mean flow. The spoiler gradient pulses and phase cycling of the RF transmitter and receiver phases are used to ensure that the desired stimulated-echo signal is accumulated preferentially. NMR velocity imaging was carried out using the proton resonance signal from water. An ISCO syringe pump established a stable water flow through the samples.

Velocity imaging using the phase-shift method

A series of velocity imaging experiments using the phase-shift method was carried out on an unconsolidated glass-bead pack and a Bentheimer sandstone sample. The 0.2-mm glass beads were packed in a cylindrical column of 2.0 cm ID, with an average porosity of 0.38. The Bentheimer sample had a diameter of 2.54 cm, a length of 4.7 cm, and a porosity of 0.23. The voxel size was $1.1\times1.1\times5$ mm^3. A number of cross-sectional images with different values of the velocity-encoding gradient was taken. The phase shift of NMR signal was calculated pixel-by-pixel and then phase-referenced to the phase with zero flow.

Figure 2 shows the phase shift as a function of the first moment of the velocity-encoding gradient, $\int t' g(t')\,dt' = G\delta\Delta$, from an image voxel for water flow in the bead pack at a constant volumetric rate of 1.5 mL/min. The measurements were made with the gradient pulse width $\delta = 2$ ms and two different observation time periods: $\Delta = 100$ and 750 ms. For an ensemble of molecules moving with a uniform velocity, the phase shift is expected to be proportional to the first moment of the gradient, and the flow velocity can be determined by a linear regression of phase vs. first moment (Caprihan et al., 1990a). Apparently, this is not the case in Figure 2, which shows a deviation from linearity as the absolute value of the first moment increases. Since the voxel size is much larger than the mean pore size, a distribution of velocities within the voxel may be expected. Consequently, the relationship between the phase shift and the mean velocity is not so straightforward.

In terms of $\langle \bar{v} \rangle_r$, Eq. 9 is rewritten as

$$S'(r,q) = \rho(r)\exp\left(iq\langle \bar{v}\rangle_r \Delta\right) \times \int_{-\infty}^{\infty} P_\Delta(\bar{v}, r)\exp\left[iq\left(\bar{v} - \langle \bar{v}\rangle_r\right)\Delta\right] d\bar{v}. \quad (11)$$

The phase shift of the measured signal is proportional to the average velocity only if the integral in Eq. 11 is a real number. For this integral to be real, the velocity distribution function must be symmetric about the mean velocity (Caprihan et al., 1990b). This is generally not true for flow through porous media. Failure to recognize this behavior may result in severe errors in the determination of velocity.

In view of the relationship in Eq. 11, it is useful to know some properties of $P_\Delta(\bar{v}, r)$ in order to interpret the results of the phase measurement of the NMR signal for fluid flow in porous media. The velocity distribution functions of water flow (16 mL/min) in the bead pack are shown in Figure 3 for

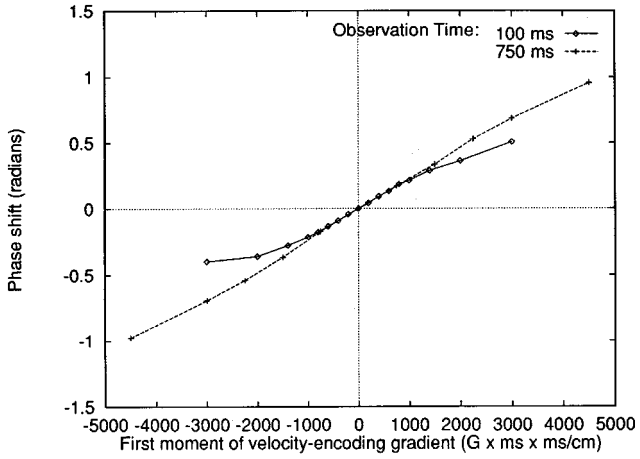

Figure 2. Phase shift from an image voxel as a function of the first moment of velocity-encoding gradient pulses for water flow at 1.5 mL/min in the 0.2-mm bead pack.

The measurements were made with two different observation times: $\Delta = 100$ and 750 ms. The pulse width $\delta = 2$ ms. The linear regime is wider for the data with longer observation time.

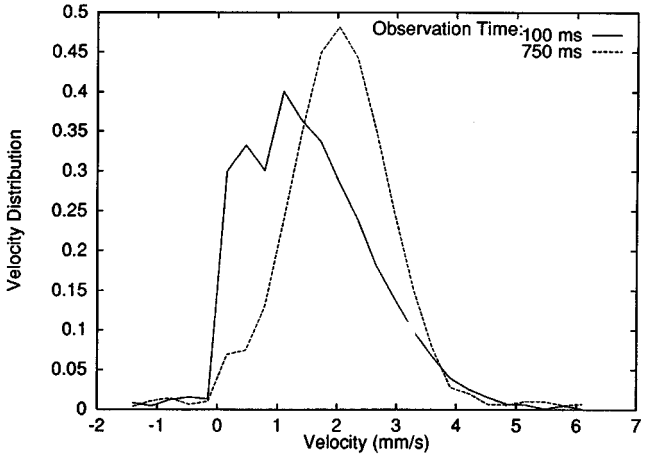

Figure 3. Velocity distributions for water flow at 16 mL/min in the 0.2-mm bead pack measured with two different observation times: 100 and 750 ms.

The width of the velocity-encoding gradient pulses was 2 ms. The shape is more symmetric for the velocity distribution measured with longer observation time.

two observation times: $\Delta = 100$ and 750 ms. The velocity distribution function is asymmetric and dominated by components of smaller velocities at short Δ, and evolves to a more symmetric shape as Δ increases. The measured $P_\Delta(\bar{v}, r)$ depicts the dynamic displacement profile for flow superimposed on diffusion during Δ. It is commonly believed that the creeping flow in irregular pores can be represented by laminar, or at least nonturbulent flow. When molecular diffusion occurs in the presence of velocity gradients, the molecule's displacement along the direction of flow is not well represented by the velocity of a single streamline, but is rather the average of many different streamlines. Based on their experimental data and computer simulations, Edwards et al. (1993) pointed out that the shape of $P_\Delta(\bar{v}, r)$ is affected by the diffusion of fluid molecules both perpendicular and parallel to flow streamlines, and is profoundly dependent on the observation time Δ. In a more recent study of Packer and Tessier (1996) and Tessier et al. (1997), the shape of the displacement probability distribution as a function of Δ was modeled in terms of laminar flow within a set of randomly oriented capillaries and computer-generated porous media. They also found that the evolution of the displacement distribution function was reproduced only when diffusion of molecules across the velocity gradients within the pore space was introduced.

The pore structure of the natural rock sample is more heterogeneous than that of the bead pack. The Bentheimer sandstone sample has a pore-size distribution ranging typically from 10 to 100 μm (Liaw et al., 1996), and it is possible that some dead-end pores may exist. The heterogeneity in pore geometry can affect the shape of the velocity distribution function. The velocity distributions measured at observation times of 300 and 500 ms for water flow at 4.8 mL/min through the Bentheimer sample are shown in Figure 4. This result indicates that much of the water is either stagnant or very slow moving. The stagnant fluid could be in nonflowing

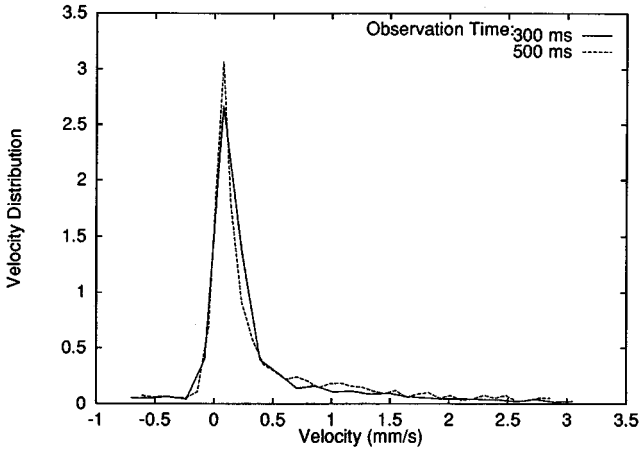

Figure 4. Velocity distributions for water flow in the cylindrical Bentheimer sandstone sample at two different observation times: 300 and 500 ms.

The pulse width of the velocity-encoding gradient was 2 ms. The flow rate was 4.8 mL/min. The shape changes little with the observation time.

pores. The shape change with the observation time in the range used in the study is not as significant as that for the bead pack.

On a macroscopic scale, one would expect to observe a constant flow in the mean flow direction despite the spatial and temporal variations of velocity for molecular motion within the pore space. The mean velocity in a voxel is estimated by expanding the phase factor of the integrand in Eq. 11 in a power series and taking the ensemble average (the integral) of each term:

$$S'(r,q) = \rho(r)\exp\left(iq\langle\bar{v}\rangle_r\Delta\right) \cdot\left\{1-\left\langle\frac{1}{2}\left[q(\bar{v}-\langle\bar{v}\rangle_r)\Delta\right]^2\right\rangle+\mathcal{O}\left(\left\langle\left[q(\bar{v}-\langle\bar{v}\rangle_r)\Delta\right]^3\right\rangle\right)\right\}. \tag{12}$$

Note that the first central moment of the velocity distribution, $\langle \bar{v} - \langle \bar{v} \rangle_r \rangle$, in the expansion vanishes according to the definition of $\langle \bar{v} \rangle_r$. The subsequent even and odd central moments affect the magnitude and phase of $S'(r, q)$, respectively. If the condition

$$q(\bar{v}-\langle\bar{v}\rangle_r)\Delta \ll 1 \tag{13}$$

is satisfied so that the higher order terms in Eq. 12 can be ignored, the phase of the signal at location r is approximated as

$$\phi(r) \simeq q\langle\bar{v}\rangle_r\Delta = \gamma(G\delta\Delta)\langle\bar{v}\rangle_r, \tag{14}$$

which is proportional to the mean velocity and the first moment of the velocity-encoding gradient. Hence, it is possible to derive a mean velocity from the linear region of each curve in Figure 2. There are two points to be noted in Figure 2. First, the mean velocity so determined is independent of Δ, although the shape of the velocity distribution is dependent on Δ. Second, the data obtained with the shorter observation time deviate from the linearity earlier as the first moment of the gradient is increased. This is consistent with the fact that the velocity distribution is more asymmetric for the shorter Δ. Figure 5 shows the cross-sectional velocity image of water flow in the bead pack obtained by a pixel-by-pixel linear regression of the data of phase vs. first moment. It gives an average velocity of 0.21 mm/s over the cross-sectional area. This value is in good agreement with the Dupuit–Forscheimer velocity (Bear, 1975), defined as the ratio of the volumetric flow rate and the product of the porosity and the cross-sectional area.

The phase shift of the NMR signal for a voxel for water flow in the Bentheimer sandstone sample at flow rates of 2 and 3.4 mL/min is plotted against the first moment of the velocity-encoding gradient, and is shown in Figure 6. The measurements were made with $\delta = 2$ ms and $\Delta = 100$ ms. For small values of the first moment where the condition in Eq. 13 is satisfied, the phase shift changes linearly with the first moment and the mean velocity determined from the slope is proportional to the flow rate. However, the phase shifts within the linear region of the curves are less than ± 0.18 radian (or $\pm 10°$), which are much smaller than those with the bead pack.

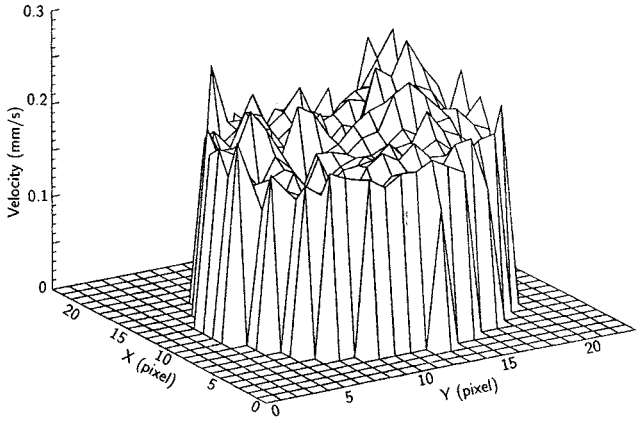

Figure 5. Cross-sectional image of velocity for water flow through the packing of 0.2-mm glass beads in a 20-mm ID cylinder.

The flow rate was 1.5 mL/min. The image resolution is 1.1 $\times$1.1 mm^2 per pixel with a slice thickness of 5 mm.

In a related study on a Texas Cream limestone sample, it was observed that the linear region of the phase shift is only within $\pm$0.09 radian. A low signal-to-noise ratio in image intensity can significantly affect the accuracy of the velocity estimation, since the smallest measurable phase shift is limited by the signal-to-noise ratio.

The phase of the NMR signal S' for a voxel is determined by

$$\phi = \arctan\left(S'_y/S'_x\right), \tag{15}$$

where S'_x and S'_y are components of the nuclear magnetization in the rotating frame. In the experiments, the two components are the amplified outputs of two nominally identical phase-sensitive detectors in the quadrature detection configuration. The estimated error of ϕ due to uncertainties in the measurements of S'_x and S'_y is given by (Bevington, 1969)

$$(\Delta\phi)^2 \simeq \left(\frac{\partial\phi}{\partial S'_x}\right)^2 (\Delta S'_x)^2 + \left(\frac{\partial\phi}{\partial S'_y}\right)^2 (\Delta S'_y)^2. \tag{16}$$

Assuming that both channels of the quadrature detection cause the same uncertainty $\Delta S'$, the estimated error in the phase becomes

$$\Delta\phi \simeq \Delta S'/S', \tag{17}$$

which is the reciprocal of the signal-to-noise ratio. The phase error could be as high as 0.05 radian even for a signal-to-noise ratio of 20, a signal sensitivity that is scarcely achieved in many velocity imaging experiments on porous media.

As the flow rate is increased, the higher-order terms in Eq. 12 become increasingly important and the range of linearity becomes smaller (see Figure 6). It would seem advantageous to measure at a smaller flow rate. In order to measure slow flow, a sufficiently large first moment of the velocity-encoding gradient has to be used to induce a measurable phase shift (Eq. 14). However, a larger first moment makes the condition in Eq. 13 more difficult to satisfy. It turns out that there exists a fundamental limitation to the estimate of flow velocity using the phase shift of the NMR signal in a voxel for heterogeneous samples.

The successful use of the phase-shift method to obtain a velocity map depends on the shape and range of the velocity distribution within each voxel, which, in turn, are influenced by the pore structure. A velocity distribution with large odd central moments, that is, more asymmetric in shape, will result in loss of phase coherence, and, hence, the measured phase shift is not related to the mean velocity. In extreme cases, the net phase shift may become too small to be effectively observed. A broad range of velocities will result in a decrease in signal intensity. As indicated in Eq. 12, the attenuation factor is primarily determined by the variance of the velocity (the second central moment). As a result of the signal loss, the accuracy of phase measurements is severely restricted. These characteristics of the velocity distribution are common for fluid flow in natural rocks.

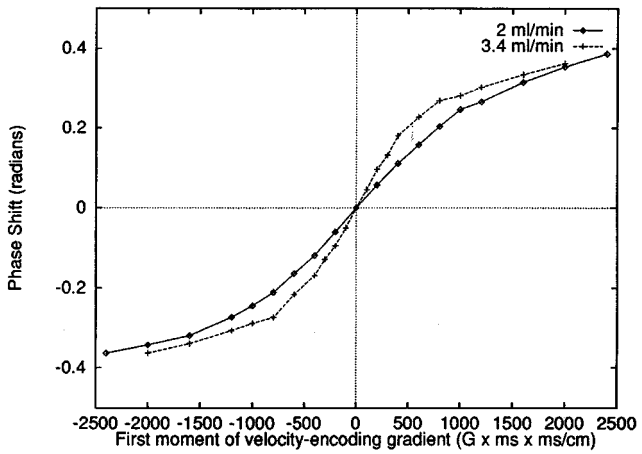

Figure 6. Phase shift of NMR signal from an image voxel as a function of the first moment of the velocity-encoding gradient for water flow in the cylindrical Bentheimer sandstone sample.

The experiments were carried out with δ = 2 ms and Δ = 100 ms at two different flow rates: 2 and 3.4 mL/min.

Velocity imaging using the velocity-distribution method

Because of the limitations of the use of the phase-shift method discussed previously, the alternative method was used to image the velocity of water flow in a Bentheimer sandstone sample. The sample is in a rectangular parallelepiped shape 50 mm long extending in the *z*-direction, 25 mm wide along the *x*-direction, and 5 mm thick in the *y*-direction. The pulse sequence shown in Figure 1 was employed to measure the spatially resolved velocity distribution from which the velocity image was reconstructed. Two sets of velocity imaging experiments were performed. The first set was carried out with a single spatial dimension plus a velocity dimension, while the second set was carried out with two spatial dimensions and a velocity dimension. These measurements were done with δ = 1.5 ms and Δ = 200 ms. The flow velocity was encoded in the range of $-$5.5 to 5.5 mm/s with 32 steps.

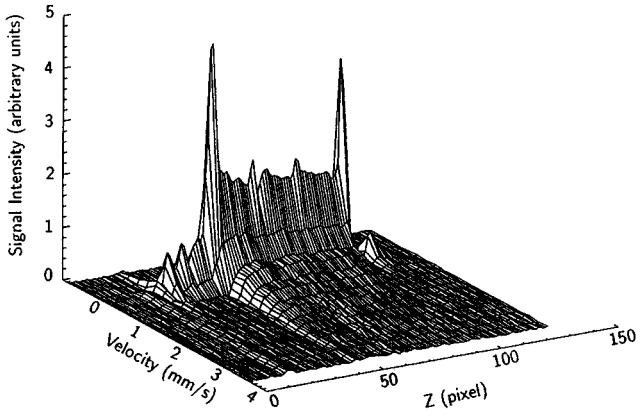

Figure 7. Joint spin-velocity density function, $\rho(z)P_\Delta(\bar{v}, z)$, as a function of position z for water flow in the rectangular Bentheimer sandstone sample.

The volumetric flow rate was 1.5 mL/min along the z-direction. The pixel size is 0.94 mm.

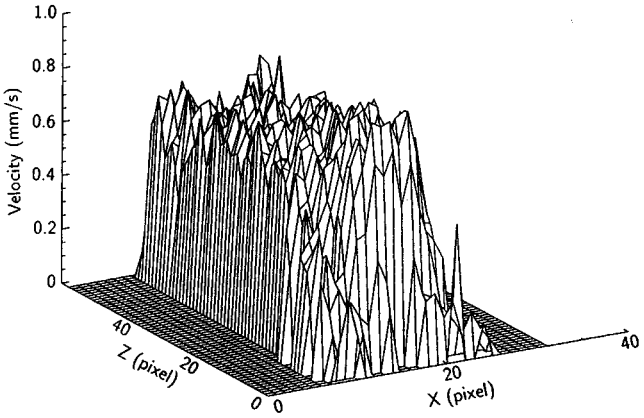

Figure 9. Longitudinal velocity image of water flow in the rectangular Bentheimer sandstone sample.

The flow rate was 1.5 mL/min. The pixel sizes are 1.56 and 0.94 mm in the x- and z-directions, respectively.

In the first set of experiments, the spatial information is frequency encoded and the velocity information is phase encoded, both in the z-direction, which corresponds to the mean flow direction. The z-dependence of the joint spin-velocity density function, that is, the product of proton density and velocity distribution, $\rho(z)P_\Delta(\bar{v}, z)$, is shown in Figure 7 for a volumetric flow rate of 1.5 mL/min. The rock sample is located between pixels $z = 40$ and 100, that is, between the two spikes resulting from free water in the end caps of the core holder. The pixel size is 0.94 mm. Note the extremely asymmetric shape of the velocity distribution in each pixel. The mean flow velocity for each pixel determined from the velocity distribution using Eq. 10 is shown in Figure 8 for two flow rates, 1.5 and 2 mL/min. As expected, these values of velocity appear to be proportional to the flow rate. In the second set of experiments, the second spatial dimension was phase encoded in the x-direction. Figure 9 shows the two-spatial-dimensional velocity image of the sample measured at a flow rate of 1.5 mL/min. The in-plane (x-z) image resolution is 1.56 mm $\times$ 0.94 mm.

The velocity distribution method provides information not only about the mean velocity but also about the dispersion processes. The knowledge of the velocity distribution enables a calculation of the variance in velocity, a parameter that is directly related to the dispersion coefficient (Seymour and Callaghan, 1997). Thus, it has the potential for investigating complex flow properties involving the interplay between hydrodynamic and structural characteristics of porous media. The cost of adding a velocity dimension to each voxel is longer experimental time. However, the experimental time is largely reduced if one of the spatial dimensions can be sacrificed.

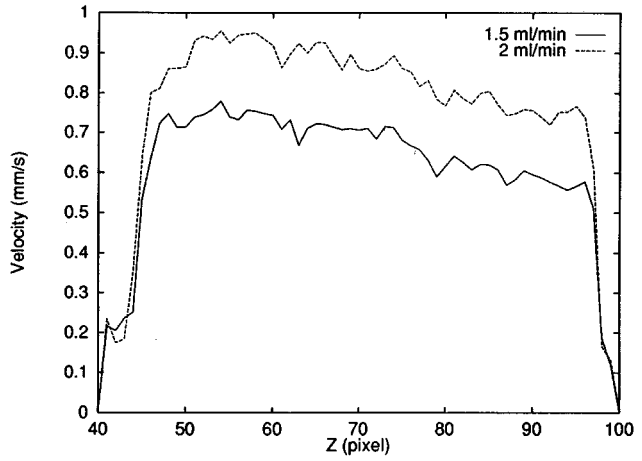

Figure 8. Longitudinal profiles of velocity for water flow along the z-direction at two different flow rates, 1.5 and 2 mL/min, in the rectangular Bentheimer sandstone sample; the pixel size is 0.94 mm.

Conclusions

We have shown that, by using appropriate pulse sequences and analysis methods, it is possible to quantitatively image the coherent flow velocity on a scale beyond the pore level in porous materials. The velocity imaging data on macroscopic scales are very important in the numerical simulations and analytical modeling of fluid transport in porous media. We have explored two different methods that make use of the phase shift and velocity distribution data, respectively, based on the PFG stimulated-echo NMR technique, to obtain velocity images of water flow in both the model and natural porous systems.

To date, most investigations on the flow velocity have used the phase-shift method. While this method may be well suited to measuring conduit flow, special case should be taken when applying it to flow in porous media. Because of the complex nature of flow in porous media, the phase shift of the NMR signal induced by the velocity-encoding gradient is not always proportional to the flow velocity. We have illustrated and dis-

cussed the conditions and limitations with respect to the estimate of a mean velocity using the phase shift. Experimental results indicate that velocity imaging using the phase-shift method for the rock sample can be more difficult than for the bead pack due to the signal's more significant loss in phase coherence.

By using the velocity-distribution method, we have been able to produce spatially resolved velocity distribution functions for water flow in a sandstone sample. Of particular importance is that the mean velocity images can be calculated from the distribution functions, even though these velocities may not be reliably obtained with the phase-shift method. In comparison with the phase-shift method, the velocity-distribution method is applicable to a wider class of media, including those exhibiting large heterogeneities in pore geometry. Moreover, this method also provides useful information about the complex hydrodynamic phenomena such as dispersion processes.

Acknowledgment

The early part of this study was carried out within the Engineering Imaging Laboratory at Texas A&M University while Dr. Carl Edwards served as Director. The authors thank him for his support and stimulating discussions.

Notation

B_0 = static magnetic field
k = wave vector conjugate to spin position
r = position vector
R = molecular displacement
S = NMR signal intensity

Literature Cited

Bear, J., *Dynamic of Fluids in Porous Media*, Academic Press, New York (1975).
Bevington, P. R., *Data Reduction and Error Analysis for the Physical Sciences*, McGraw-Hill, New York (1969).
Callaghan, P. T., *Principles of Nuclear Magnetic Resonance Microscopy*, Clarendon, Oxford (1991).
Callaghan, P. T., K. R. Jeffrey, and Y. Xia, ''Translational Motion Imaging with Pulsed Gradient Spin Echo Methods,'' *Magnetic Resonance Microscopy*, B. Blumich and W. Kuhn, eds., VCH, Weinheim (1992).
Caprihan, A., R. H. Griffey, and E. Fukushima, ''Velocity Imaging of Slow Coherent Flows Using Stimulated Echoes,'' *Magn. Reson. Med.*, **15**, 327 (1990a).
Caprihan, A., S. A. Altobelli, and E. Benitez-Read, ''Flow-Velocity Imaging from Linear Regression of Phase Images with Techniques for Reducing Eddy-Current Effects,'' *J. Magn. Reson.*, **90**, 71 (1990b).
Edwards, C. M., C. T. Chang, and S. Sarkar, ''The Measurement of Fluid Velocities in Porous Media,'' *Proc. Society of Core Analysts Technical Conf.*, Society of Core Analysts (1993).
Gleeson, J. W., and D. E. Woessner, ''Three-Dimensional and Flow-Weighted NMR Imaging of Pore Connectivity in a Limestone,'' *Magn. Reson. Imaging*, **9**, 879 (1991).
Kulkarni, R., A. T. Watson, J. E. Nordtvedt, and A. Sylte, ''Two-Phase Flow in Porous Media: Property Identification and Model Validation,'' *AIChE J.*, **44**, 2337 (1998).
Kutsovsky, Y. E., L. E. Scriven, H. T. Davis, and B. E Hammer, ''NMR Imaging of Velocity Profiles and Velocity Distributions in Bead Packs,'' *Phys. Fluids*, **8**(4), 863 (1996).
Lebon, L., L. Oger, J. Leblond, and J. P. Hulin, ''Pulsed Gradient NMR Measurements and Numerical Simulation of Flow Velocity Distribution in Sphere Packings,'' *Phys. Fluids*, **8**(2), 293 (1996).
Liaw, H.-K., R. Kulkarni, S. Chen, and A. T. Watson, ''Characterization of Fluid Distributions in Porous Media by NMR Techniques,'' *AIChE J.*, **42**, 538 (1996).
Lu, X., G. P. Pepin, R. M. Moss, M. Semmelbeck, P. Miao, and A. T. Watson, ''X-Ray Computed Tomography Studies of Gas Storage and Transport in Devonian Shales,'' *AIChE J.*, **40**(7), 1246 (1994).
Merrill, M. R., ''Local Velocity and Porosity Measurements Inside Casper Sandstone Using MRI,'' *AIChE J.*, **40**(7), 1262 (1994).
Moran, P. R., ''A Flow Velocity Zeugmatographic Interlace for NMR Imaging in Human Body,'' *Magn. Reson. Imaging*, **1**, 197 (1982).
Nesbitt, G. J., T. W. Fens, J. S. van den Brink, and N. Roberts, ''Evaluation of Fluid Displacement in Porous Media Using NMR Microscopy,'' *Magnetic Resonance Microscopy*, B. Blumich and W. Kuhn, eds., VCH, Weinheim (1992).
Packer, K. J., and J. J. Tessier, ''The Characterization of Fluid Transport in Porous Solid by Pulsed Gradient Stimulated Echo NMR,'' *Mol. Phys.*, **87**, 267 (1996).
Slattery, J. C., *Momentum, Energy, and Mass Transfer in Continua*, Krieger, New York (1981).
Seymour, J. D., and P. T. Callaghan, ''Generalized Approach to NMR Analysis of Flow and Dispersion in Porous Media,'' *AIChE J.*, **43**, 2096 (1997).
Tessier, J. J., K. J. Packer, J.-F. Thovert, and P. M. Adler, ''NMR Measurements and Numerical Simulation of Fluid Transport in Porous Solids,'' *AIChE J.*, **43**, 1653 (1997).
Watson, A. T., and C. T. P. Chang, ''Characterizing Porous Media with NMR Methods,'' *Prog. in Nucl. Mag. Res. Spect.*, **31**, 343 (1997).

Manuscript received Sept. 3, 1998, and revision received Jan. 7, 1999.